Measurement of surface temperature of weld pools by infrared two colour pyrometry

K. Yamazaki*, E. Yamamoto, K. Suzuki, F. Koshiishi, S. Tashiro, M. Tanaka and K. Nakata

In this research, two colour pyrometry was conducted to obtain the surface temperature of weld pools, in which the weld pool was photographed by a high speed camera during arc welding. Two wavelengths (950 and 980 nm) of light in the infrared range were selected from the thermal radiation light emitted from the weld pool at the instant when the arc was extinguished, using an imaging spectroscope. Consequently, in gas tungsten arc welding, it was shown that the surface temperature distribution of a weld pool is affected by the sulphur content in the base metal. It is thought that this temperature distribution is determined by the balance between the driving forces of viscous drag from the cathode jet of plasma and Marangoni surface tension. In gas metal arc welding, it was seen that the surface temperature distribution becomes uniform and the temperature is 1715–1845 K, which is obviously lower than that of the metal droplet.

Keywords: Weld pool temperature, Two colour pyrometry, GTA welding, GMA welding, Sulphur, Convection

Introduction

Knowing the temperature of the weld pool in arc welding is important to understand arc phenomena and metallurgical reactions. Thermocouples have been used to record the welding thermal cycle for experimental purposes.[1–3] However, the temperature measurement by contact sensors such as a thermocouple may cause a risk of disturbing the temperature field and the convection of a weld pool. In addition, the temperatures have to be measured in many locations in order to obtain the temperature distribution and thus troublesome work of fixing sensors becomes inevitable. By contrast, non-contact temperature measurement by radiation thermometry is advantageous in obtaining the surface temperature distribution without influencing the temperature of a measured object. The temperature of a weld pool, mainly in gas tungsten arc (GTA) welding, has been measured by radiation thermometry. Sato *et al.* reported temperature measurement by ultraviolet radiation thermometry.[4] However, the temperature measurement has been limited only from the backside of a baseplate in order to avoid the disturbance by the radiation light from the arc plasma and the tungsten electrode. Giedt *et al.*[5] and Okagaito *et al.*[6] attempted to measure the temperature of a weld pool from the surface side by radiation thermometry by moving the welding torch (tungsten electrode) outside the measuring area as soon as the welding current is turned off. In these studies, there was a time lag of ~ 50 ms between turning off the current and starting temperature measurement. As a result, the temperature at the start of measurement was lower than that of the moment when the arc was extinguished.

Using two colour pyrometry, the authors measured the temperature of molten droplets in gas metal arc (GMA) welding right after extinguishing the welding arc.[7] In this measurement, two wavelengths of 950 and 980 nm in the infrared range were selected to sufficiently lower the effect of the arc plasma and the current waveform was controlled to decrease the welding current instantaneously from the level at the measuring time. In the present research, the authors measured the temperature distribution on the surface of a weld pool at the moment of extinguishing the welding arc using infrared two colour pyrometry. The measurement was made in not only GTA welding but also in GMA welding. There have been few reports concerning the temperature measurement in GMA welding. In the GTA welding, Ar and He were used as the shielding gas and the effect of the sulphur content of the base metal on the temperature distribution on the weld pool surface was investigated. In the GMA welding, the weld pool surface temperatures were compared between CO_2 arc welding and metal active gas (MAG, Ar–20%CO_2) arc welding at the same welding currents.

Measurement method

Principles of two colour pyrometry

Two colour pyrometry is a temperature measurement method that selects two different wavelengths of light emitted from a measured object. It determines the temperature from the ratio of radiation intensity of two lights, under the condition that the radiation emissivity can be regarded as constant within closely different

Kobe Steel, Ltd, Welding Company, 100-1 Miyamae, Fujisawa, Kanagawa 251 8551, Japan

*Corresponding author, email yamazaki.kei@kobelco.com

Published by Maney on behalf of the Institute
Received 10 June 2009; accepted 22 September 2009
DOI 10.1179/136217109X12537145658814

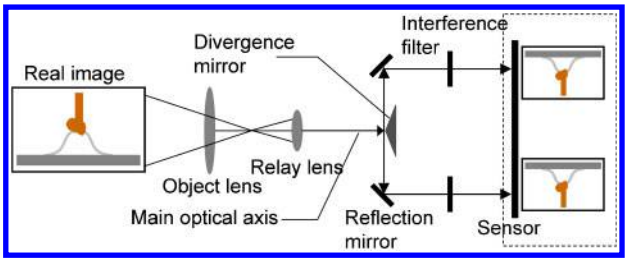

1 Optical system of two colour pyrometry

wavelengths. The following equation is the ratio of radiation intensity which is obtained by substituting the wavelength and radiation emissivity into Plank's radiation law

$$\frac{I_1}{I_2}=\frac{\varepsilon_2}{\varepsilon_1}\left(\frac{\lambda_2}{\lambda_1}\right)^5\frac{1-\exp(C_b/\lambda_2 T)}{1-\exp(C_b/\lambda_1 T)} \quad (1)$$

where I_1, I_2 are radiation intensities (W m^{-3} sr^{-1}); ε_1, ε_2 are emissivities; λ_1, λ_2 are wavelengths (nm); C_b= 0·014388 mK; and T is temperature (K). When Wien's approximation is applied and the emissivity is assumed not to differ within the selected wave lengths, equation (1) becomes equation (2)

$$\frac{I_1}{I_2}=\left(\frac{\lambda_2}{\lambda_1}\right)^5\frac{\exp(C_b/\lambda_2 T)}{\exp(C_b/\lambda_1 T)} \quad (2)$$

From this formula, a temperature, T can be expressed by the following formula; that is, the temperature of the object can be derived from the radiation intensity ratio of the two wavelengths of light.

$$T=\frac{C_b(\lambda_1-\lambda_2)}{\lambda_1\lambda_2}\frac{1}{\ln\left(I_1{\lambda_1}^5/I_2{\lambda_2}^5\right)} \quad (3)$$

Although two colour pyrometry and spectropyrometer based multiwavelength are well known as a non-contact type thermometry without requiring material emissivity, it is especially easy for two colour pyrometry to visualise two-dimensional temperature field of molten metal in real time by combining with high speed camera because of simplicity of that optical system.

Experimental apparatus for two colour pyrometry

A schematic diagram of the optical system of the experimental apparatus is shown in Fig. 1. With this system, the thermal emission light emitted from a high temperature object is divided by an imaging spectroscope (multispectral imager by Photron) after passing through the object lens. The divided light passes through the two interference filters of different wavelengths (midwavelength: 950 and 980 nm) and forms an image on the element screen of a high speed digital camera (FASTCAM-512PCI by Photron). Then, the image is recorded. In this experiment, the image data of two wavelengths taken by the high speed camera was converted to Microsoft Excel data, using an image analysing software (Dipp-Macro by Ditect) to accurately adjust the positions of images on the Excel window. Also the temperature had to be corrected considering the characteristics of the camera and lenses. For this purpose the pyrometry system was calibrated by comparing the temperature obtained from the strength ratio of the two waves of light and the actual

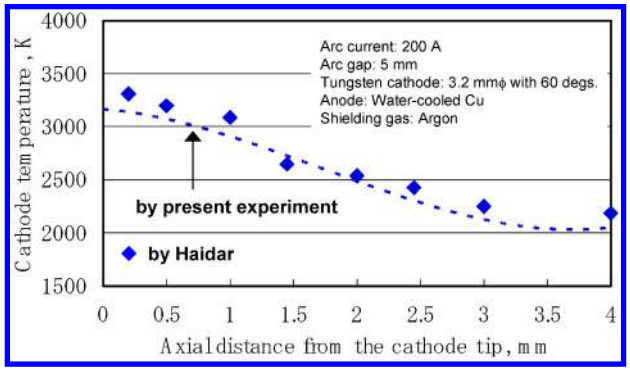

2 Distribution of tungsten electrode surface temperature measured by two colour pyrometry

temperature (max. 3200 K) obtained by measuring the radiant temperature of the tungsten lamp calibrated by Japan Calibration Service System as a standard lamp. The temperature data was calculated from the radiation intensity ratio data for each pixel referring to this calibration data. It is well known that the radiation light from arc plasma concentrates in 200 to 400 nm wavelength in the ultraviolet ray range and is weak in the infrared ray range. With the two wavelengths of 950 and 980 nm selected in this measuring system, the effect of the plasma radiation could be reduced considerably when compared with the ultraviolet ray range and the visible ray range.

Haidar *et al.* succeeded in accurately measuring the surface temperature of the tungsten electrode in GTA welding by using a large spectral apparatus (focal length of 1 m) and an optical mirror and lens system.[8] In order to evaluate the reliability of the infrared two colour pyrometry apparatus in this study, the surface temperature of the tungsten electrode in GTA welding was measured and compared with the result reported by Haidar *et al.* The cathode image was recorded just after extinguishing the arc from the steady state (arc current of 200 A) at a recording speed of 500 frames/s. Our experimental result of the cathode surface temperature distribution was shown in Fig. 2. For comparison, the temperature measured by Haidar *et al.* was also plotted. As a result, the temperature measurements obtained by the two colour pyrometry apparatus have agreed substantially with those reported by Haidar *et al.* It is suggested that the measured temperature does not differ from that at the arcing electrode within 2 ms (the maximum time lag at a recoding speed of 500 fames/s) after extinguishing the arc. The accuracy of temperature measurement ($\Delta T/T$) of the two colour pyrometry apparatus in this study is assumed about $\pm 5\%$ because it is reported that the temperature fluctuates by 100 K around the electrode tip heated over 3000 K.

Measurement of temperature of GTA weld pools

Testing materials

Chemical compositions of the base metals used in this study are shown in Table 1. Two kinds of SUS304 stainless steel plates containing 10 and 250 ppm sulphur were used. The SUS304 stainless steel plate containing 10 ppm sulphur is designated as 'the LS plate', and that containing 250 ppm sulphur is designated as 'the HS

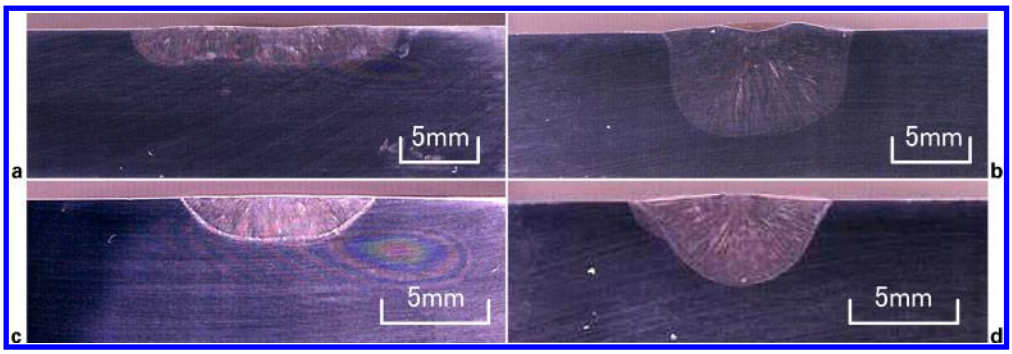

a He shielded, LS; *b* He shielded, HS; *c* Ar shielded, LS; *d* Ar shielded, HS

3 Effect of sulphur content on penetration shape in GTA welding using Ar or He for shielding gas (arc current: 150 A; arc gap: 6 mm; arc time: 20 s)

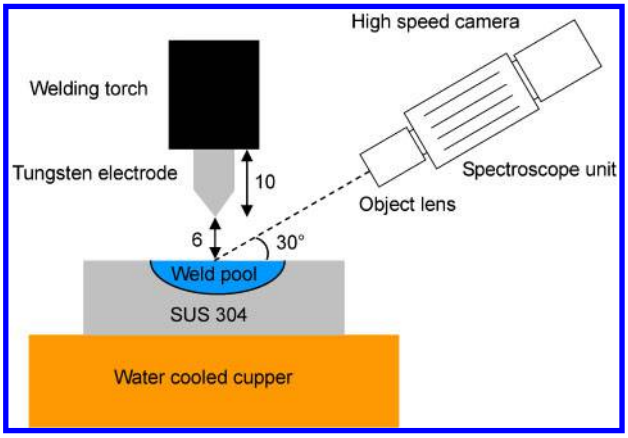

4 Arrangement of experimental apparatus

plate'. The LS and HS plates were welded using Ar or He for the shielding gas. Their weld penetrations are shown in Fig. 3. In GTA welding, it is known that the penetration is affected noticeably by the sulphur content of the base metal.[9] As shown in the figure, it was confirmed that the deeper penetration resulted in the HS plates than in the LS plate for both shielding gases.

Experimental methodology

A stationary GTA arc was generated on the base metal of SUS304 set on a water cooled Cu plate under the condition of the tungsten electrode extension of 10 mm, arc length of 6 mm, arc current of 150 A, and shielding gas of Ar or He. The welding current was turned off to extinguish the arc immediately after the 20 s arcing period and the arc images were recorded by a high speed camera before and after the instant when the arc was extinguished. Among the images, that showing the instant when the arc was completely extinguished was selected to measure the temperature of the weld pool. To prevent the tungsten electrode image from being projected onto the central part of a weld pool image, the weld pool was photographed from the upper direction 60° inclined against the perpendicular line. The experimental apparatus arrangement is schematically shown in Fig. 4. The spatial resolution of image data is about 50 μm/pixel. The shutter speed was adjusted to the 8 ms exposure per frame to obtain the sufficient radiation from the weld pool.

Table 1 Chemical compositions of base metals, wt-%

	C	Si	Mn	P	S	Ni	Cr
LS	0·07	0·3	0·9	0·03	0·001	8·2	18·2
HS	0·07	0·3	1·1	0·04	0·025	8·1	18·1

Results of experiment

The 950 nm wavelength images of the weld pools and the surface temperature distribution maps obtained by the infrared two colour pyrometry are shown in Fig. 5. Figure 5*a*, *b* and *d* shows the image of the tungsten electrode projected in the lower part of each photo of the weld pool, while the electrode was not projected in Fig. 5*c* that was taken in Ar shielded GTA welding on the LS plate. The arc pressure in Ar shielded GTA welding is known to be higher than that in He shielded GTA welding.[10] Therefore, in Ar shielded GTA welding on the LS plate, the high arc pressure probably pushed down the weld pool surface over the large area below the base metal surface even after extinguishing the arc. It can be thus considered that the radiant light from the tungsten electrode was reflected inside the swelled edge of the weld pool and was not observed by the camera placed in the 60° inclined direction. By contrast, it can be assumed that, in He or Ar shielded GTA welding on the HS plate, the weld pool surface was somewhat pushed down in the central area, but the weld pool surface was approximately flat at the pool edges. It was concluded that the radiant light from the tungsten electrode did not affect the central area of the weld pool.

From the surface temperature distribution maps shown in Fig. 5, it is obvious that the highest temperature area exists near the centre of the weld pool, and that the temperature decreases toward the edge of the weld pool. Furthermore, the surface temperature distribution was likely to change depending on the type of the shielding gas and the base metal. Figure 6 shows the surface temperature distributions in the radial direction from the centre to the edge of the weld pool. In He shielded GTA welding, as shown in Fig. 6*a*, the surface temperature of the weld pool on the HS plate is ~2900 K at the centre and it abruptly drops to ~1900 K in the region only 1 to 2 mm apart from the centre. In contrast to this, the surface temperature of the weld pool on the LS plate is ~2300 K at the centre, which is lower than that on the HS plate, and it decreases gradually toward the edge. In Ar shielded GTA welding, as shown in Fig. 6*b*, the surface temperature at the centre of the weld pool is lower than that in He shielded GTA welding. This is presumably because the total heat input and the heat input density in Ar shielded GTA welding is lower than that in He

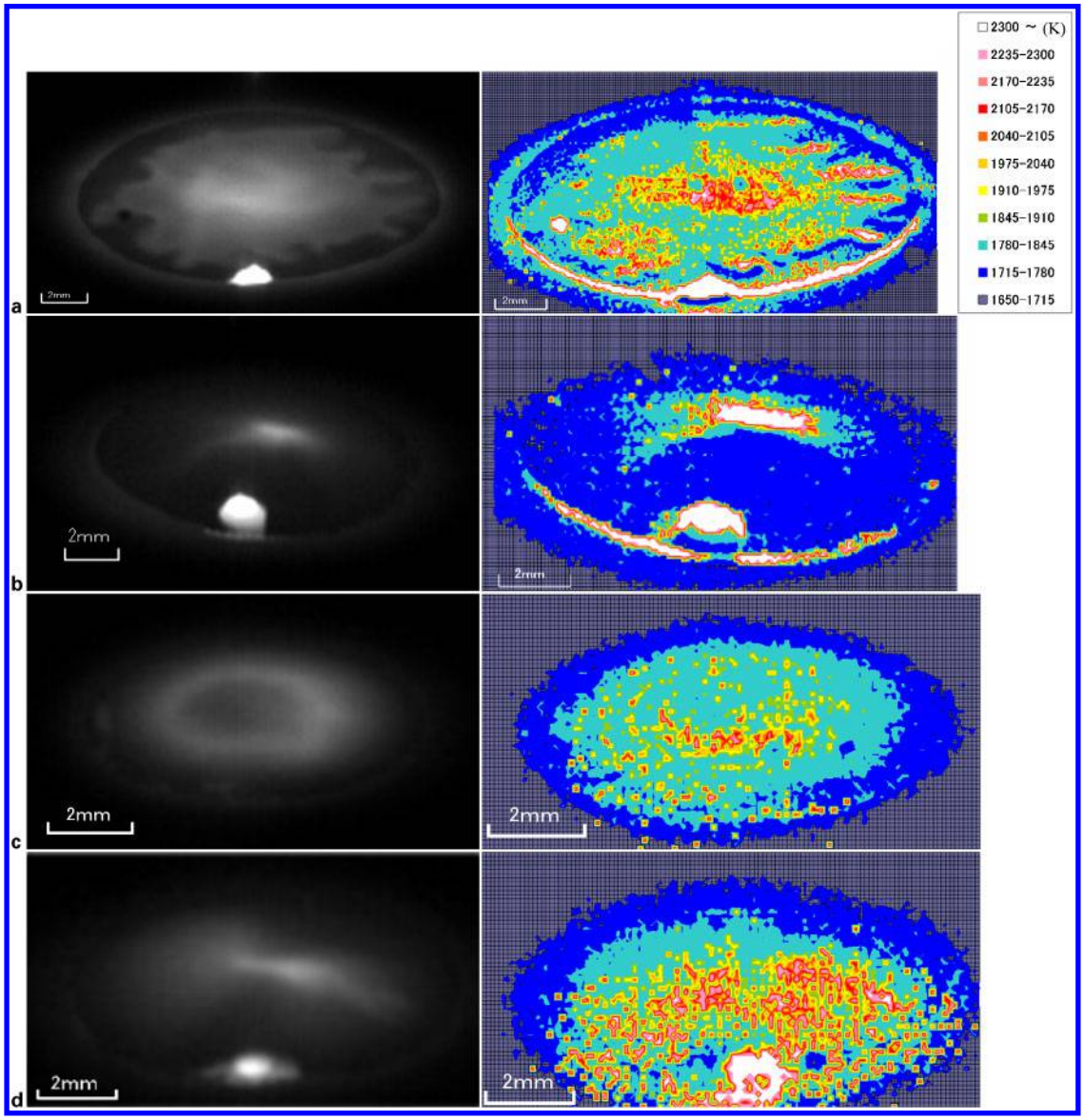

a He shielded, LS; *b* He shielded, HS; *c* Ar shielded, LS; *d* Ar shielded, HS

5 Surface temperature distribution maps of weld pools immediately after arc is extinguished in GTA welding (base metal: SUS304; welding current: 150 A; arc length: 6 mm)

shielded GTA welding.[11] In Ar shielded GTA welding on the HS plate, the temperature distribution is unique, that is, the temperature is higher in the region 1 to 2 mm apart from the centre than at the centre.

Although the highest temperature values fluctuate a little, these differences in the surface temperature distribution depending on the sulphur content of the base metal are highly repeatable. They are assumed to strongly correlate with the convection on the molten weld pool surface.

Surface temperature and convection of weld pool

A relatively high concentration of surface active elements such as oxygen and sulphur in the base metal increases weld penetrations. Heiple *et al.*[12] explained this phenomenon by a following mechanism: the surface active element reverses the temperature gradient of surface tension and a force driven by the difference in surface tension reverses the Marangoni convection in the molten weld pool. Also, Sahoo *et al.*[13] indicated that calculation of temperature gradient of surface tension in Fe–O and Fe–S systems can change from a positive value at relatively low temperature to a negative value at high temperature when oxygen and sulphur is high concentrations. In light of this mechanism, the authors discuss the behaviour of the molten weld pool convection estimated by the measured temperature field of the molten pool.

In the experiment of He shielded GTA welding on the HS plate, the temperature at the centre of the weld pool surface was $\sim$2900 K and it dropped to $\sim$1900 K in the region only 1 to 2 mm apart from the centre. This can probably be explained in such that the molten pool flows inward at the surface, the hot molten metal heated by the arc at the centre moves toward the bottom, and it is cooled down to almost the melting temperature when it rises back to the off-centre surface. The heat transfer during this convection process can be considered to cause the deep penetration in He shielded GTA welding on the HS plate. In He shielded GTA welding on the LS plate, the weld penetration became wide and shallow.

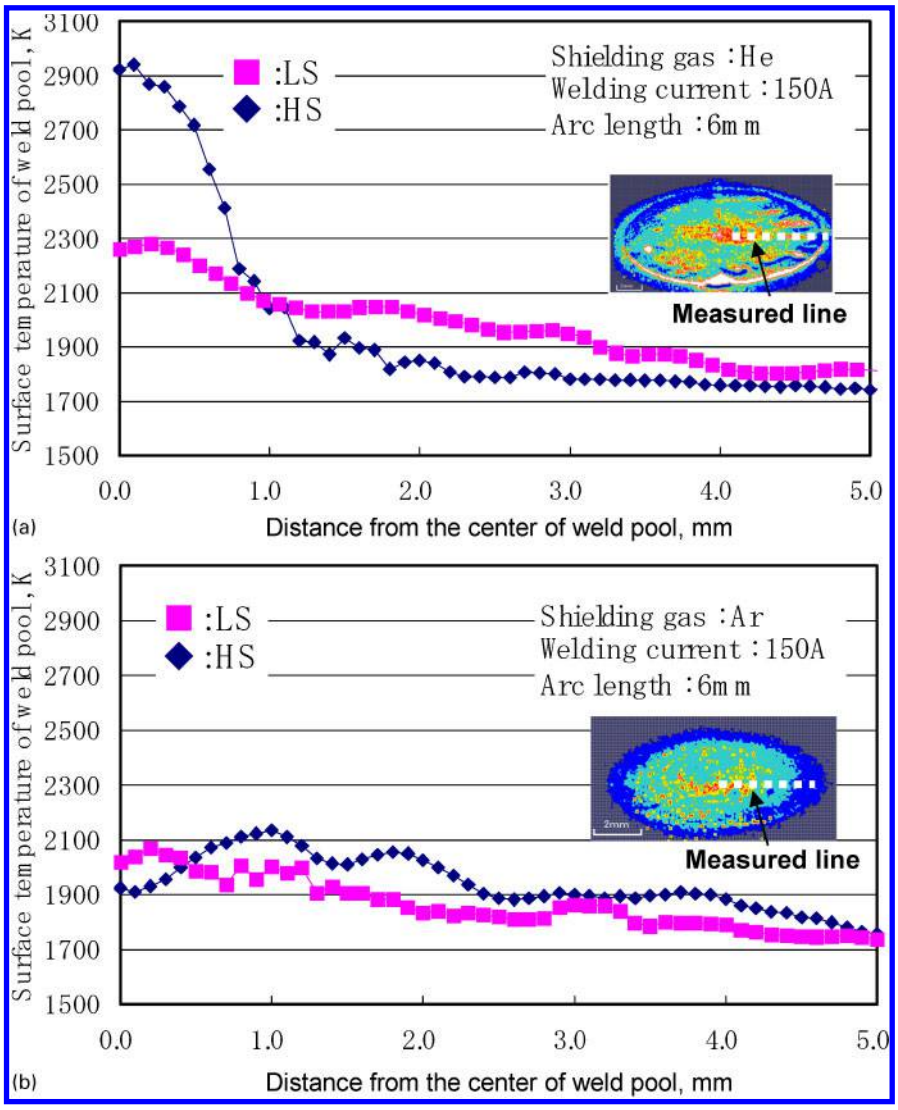

a shielding gas: He; *b* shielding gas: Ar

6 Surface temperature distributions along weld pool centreline

The temperature of the weld pool centre measured in this experiment was ~2300 K which was lower than that on the HS plate and the temperature decreased gradually toward the edge. This can be explained in such that the weld pool flows outward from the centre on the surface and it is transferred together with its heat in the radial direction.

In Ar shielded GTA welding on the HS plate, a unique temperature distribution was recorded. That is, the temperature was higher in the region 1 to 2 mm apart from the centre than at the weld pool centre. This is presumably caused by the complicated interference of the inward Marangoni force and the outward shearing force of the plasma stream. This phenomenon is explained by Tanaka *et al.* by using the numerical calculation results as follows:[14] the plasma stream stagnates at the weld pool centre, and a low speed of the plasma flow and the weak shearing force result there. At the weld pool edge, the flow speed of the plasma stream also lowers and the outward shearing force decrease. Consequently, the Marangoni force at the centre and edge becomes dominant, causing an inward flow in the weld pool. In the mid area between the centre and the edge, the shearing force of ~50 Pa in the maximum induced by the plasma stream becomes dominant, causing an outward flow. At the area (1 to 2 mm apart from the centre) where the outward and inward flows meet, the temperature becomes slightly higher than that in the weld pool centre.

Measurement of temperature of GMA weld pools

Experimental method

The experimental apparatus is schematically shown in Fig. 7. In this apparatus, a welding current with an intended waveform can be output by inputting an arbitrary waveform into the transistor regulated power source. The external characteristic of the power source was set up in a constant current mode and the DCEP polarity was used. The wire feed speed was controlled by a feeding system independent of the power source. A 1·2 mm diameter solid wire corresponding to JIS (Japan Industry Standard) Z 3312 YGW12 was used for the welding wire, and 100%CO_2 and Ar–20%CO_2 (MAG) were used individually for the shielding gas. JIS SM490 A steel plates were used for the base metal. The average welding current was 280 A, the welding

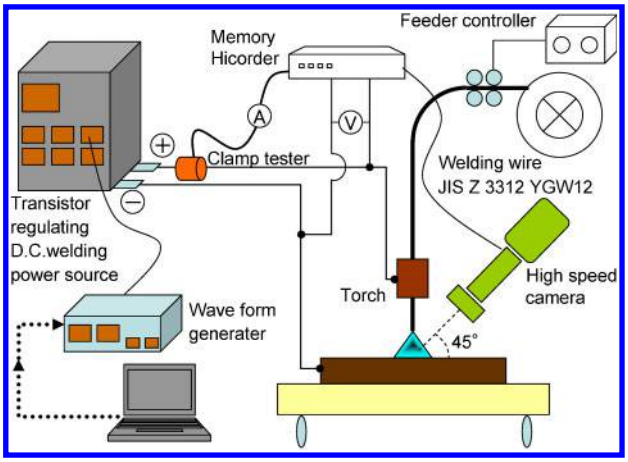

7 **Overall experimental apparatus including power source and waveform controller**

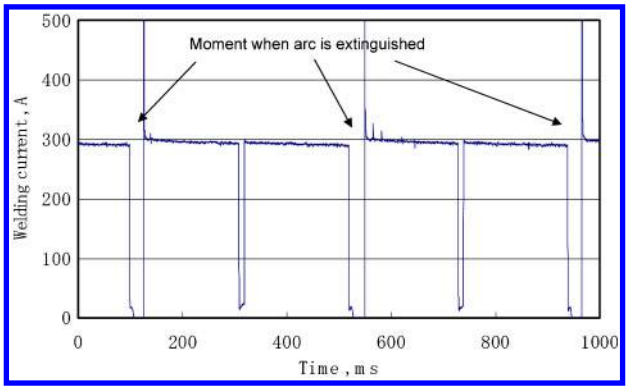

8 **Waveform of welding current (wire: JIS Z3312 YGW12; φ: 1·2 mm; welding speed: 5 mm s^{-1}; wire feed rate: 9·5 m min^{-1}; welding current: 280 A; shielding gas: 80Ar–20CO$_2$; distance between tip and base metal: 25 mm)**

speed was 5 mm s^{-1}, and the contact tip to base metal distance was 25 mm. When the weld pool is exposed to the arc, it is difficult to measure the temperature on the weld pool surface accurately. To overcome this problem, the welding current was switched instantaneously from the measuring current to a low current (0 to 40 A) by the waveform controllable at 5 Hz and immediately after extinguishing the arc, the surface temperature of the weld pool was measured. The typical welding current waveform is shown in Fig. 8. A high speed camera was set in a 45° inclined position against the weld pool. To obtain sufficient radiant light from the weld pool, the exposure time per frame was set at 8 ms as same as that in GTA welding.

Measurements of surface temperature of weld pools in MAG (Ar–20%CO$_2$) welding

Figure 9 shows a 950 nm wavelength image of the weld pool and its surface temperature distribution measured by the infrared two colour pyrometry, immediately after extinguishing the arc. The surface temperature of the weld pool ranges from 1715 to 1845 K showing a relatively flat distribution. This temperature level is obviously lower than that of the molten metal droplet measured by the same system.[7] This is presumably because the convection speed inside the weld pool and on its surface is considerably high, and thus the energy fed by the arc is transferred backward rapidly in the weld pool because of a high speed flow. For instance, in Fig. 9, there are high temperature regions near both sides of the weld pool ~7 mm away from the front edge of the weld pool (~3 mm away from the point just beneath the arc). The region that is assumed to be just beneath the arc shows a lower temperature than the edge. This is probably because the high temperature molten metal immediately beneath the arc was pushed backward rapidly by a high speed plasma stream. That is, the degree of arc induced overheating of the weld pool was relatively low. In contrast to this, Fig. 10 shows how the temperature distribution changed for a short time after an overheated metal droplet dropped onto the weld pool. The average temperature of a molten metal droplet in MAG welding was ~2300 K under the same welding conditions. At the moment when the high temperature droplet dropped onto the weld pool, the surface temperature of the droplet sunk area shown by a dotted circle in Fig. 10*a* increased instantaneously. Then the molten metal and heat were pushed backward by the weld pool convection, resulting in an almost flat distribution of the surface temperature 8 ms after the droplet fell as shown in Fig. 10*b*.

Measurements of surface temperature of weld pool in CO$_2$ arc welding

Figure 11 shows a 950 nm wavelength image of the weld pool and its surface temperature distribution measured by the infrared two colour pyrometry, immediately after extinguishing the arc in CO$_2$ arc welding. The surface temperature distribution is relatively flat similar to that

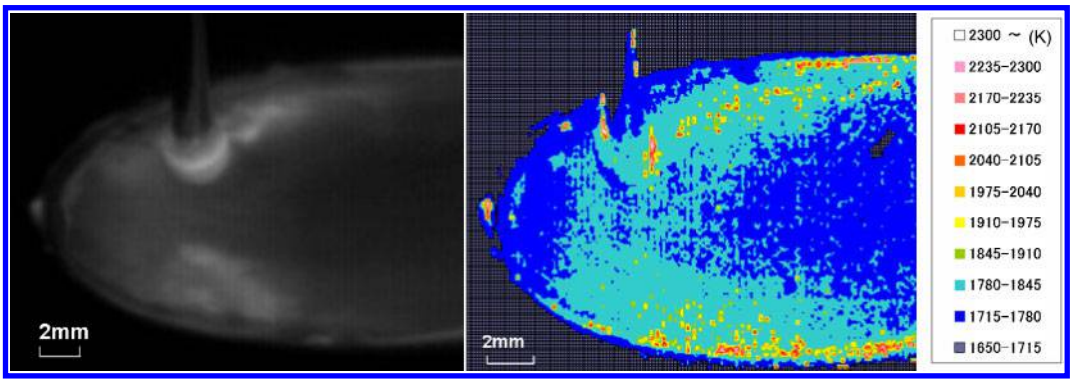

9 **Surface temperature distribution map of weld pool immediately after arc is extinguished in MAG welding (wire: JIS Z3312 YGW12; φ: 1·2 mm; welding speed: 5 mm s^{-1}; wire feed rate: 9·5 m min^{-1}; welding current: 280 A; shielding gas: 80Ar–20CO$_2$; distance between tip and base metal: 25 mm)**

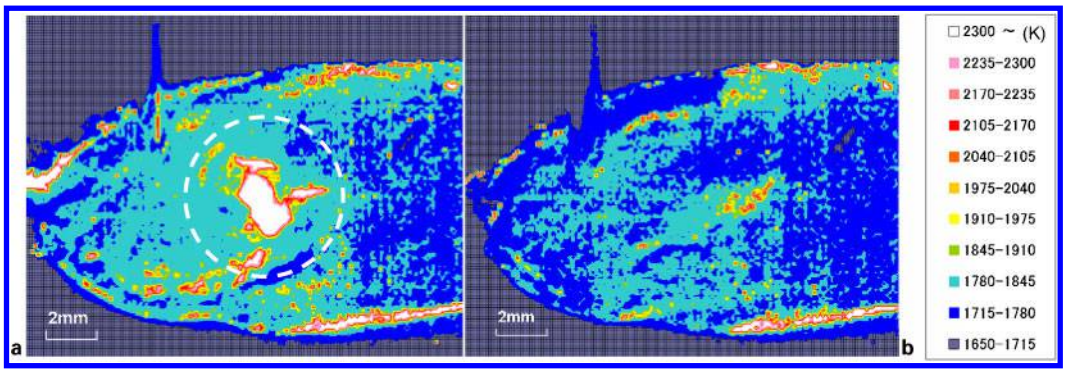

a at the moment when arc is extinguished; *b* 8 ms after arc is extinguished

10 Surface temperature distribution maps when molten droplet dropped into weld pool in MAG welding (wire: JIS Z3312 YGW12; φ: 1·2 mm; welding speed: 5 mm s^{-1}; wire feed rate: 9·5 m min^{-1}; welding current: 280 A; shielding gas: 80Ar–20CO_2; distance between tip and base metal: 25 mm)

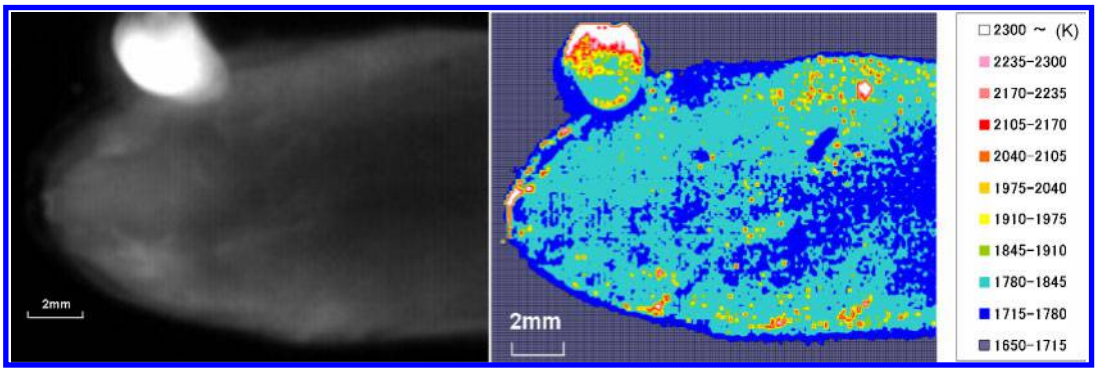

11 Surface temperature distribution map of weld pool immediately after arc is extinguished in CO_2 welding (wire: JIS Z3312 YGW12; φ: 1·2 mm; welding speed: 5 mm s^{-1}; wire feed rate: 10·2 m min^{-1}; welding current: 280 A; shielding gas: 100%CO_2; distance between tip and base metal: 25 mm)

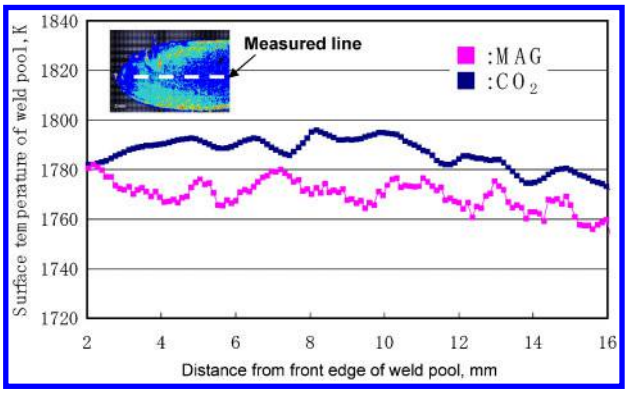

12 Surface temperature distributions along weld pool centreline (wire: JIS Z3312 YGW12; φ: 1·2 mm; welding speed: 5 mm s^{-1}; welding current: 280 A; distance between tip and base metal: 25 mm)

shown in Fig. 9 obtained in MAG welding in the same welding current, but the temperature ranges mostly from 1780 to 1845 K, slightly higher than in MAG welding. In addition, in the backward part of the weld pool, not in an area immediately beneath the arc, high temperature regions were observed on both sides, as observed in MAG welding. Figure 12 shows the surface temperature transition along the centreline of the weld pool in the welding direction. It can be considered that, in CO_2 arc welding, the arc is constricted by the thermal pinch effect, and thus the surface temperature becomes slightly higher than in MAG welding.

Conclusions

In this research, an experimental apparatus of two colour pyrometry was set up using infrared wavelengths of 950 and 980 nm to measure the surface temperature distribution of weld pools in GTA welding and GMA welding. The test results are summarised in the following.

1. In stationary He shielded GTA welding, the surface temperature of the weld pool made on the HS (high sulphur) plate was ~2900 K at the centre of the weld pool and dropped to ~1900 K in the region only 1 to 2 mm apart from the centre. By contrast, the surface temperature of the weld pool made on the LS plate was ~2300 K at the centre of the weld pool, which was lower than that on the HS plate, and decreased gradually toward the edge of the weld pool.

2. In stationary Ar shielded GTA welding, the surface temperature at the centre of the weld pool was lower than that in He shielded GTA welding. In Ar shielded GTA welding on the HS plate, such a unique surface temperature distribution that the areas 1 to 2 mm apart from the centre recorded a higher temperature than that at the centre of the weld pool was observed.

3. It can be assumed that the direction of the molten metal flow on the weld pool surface is affected by the sulphur content of the base metal; and that the balance between the molten metal flow and the outward shearing force induced by the plasma stream affects the surface temperature distribution and the penetration profile.

4. In GMA welding, the weld pool surface temperature distribution was relatively flat, which was obviously lower than that of a metal droplet measured by the same measuring system.

5. In GMA welding, the surface temperature distribution of the weld pool confirmed that high temperature regions existed at both sides in the backward part of the weld pool. This is presumably because the thermal energy transferred from the arc is conveyed rapidly toward the backward part of the weld pool by a high speed flow of molten metal.

6. The surface temperature of the weld pool in CO_2 arc welding was apt to be somewhat higher than that in MAG welding. This is probably because the arc was constricted by the thermal pinch effect.

References

1. M. Inagaki, T. Wada and M. Uda: *J. Jpn Weld. Soc.*, 1965, **34**, (3), 322.
2. T. Hashimoto and F. Matsuda: *J. Jpn Weld. Soc.*, 1965, **34**, (7), 654.
3. T. Yamamoto, Y. Yamazaki, Y. Tsuji, F. Miyasaka and T. Ohji: *Q. J. Jpn Weld. Soc.*, 2005, **23**, (1), 71.
4. T. Sato, A. Ohkubo, T. Ohji and Y. Hirata: *Q. J. Jpn Weld. Soc.*, 1997, **15**, (4), 631.
5. W. H. Giedt, X.-C. Wei and S.-R. Wei: *Weld. J.*, 1984, **63**, (12), 376s.
6. T. Okagaito, T. Ohji, and Y. Hirata: *Q. J. Jpn Weld. Soc.*, 2004, **22**, (1), 21.
7. K. Yamazaki, E. Yamamoto, K. Suzuki, F. Koshiishi, K. Waki, S. Tashiro, M. Tanaka and K. Nakata: *Q. J. Jpn Weld. Soc.*, 2008, **26**, (3), 214.
8. J. Haidar and A. J. D. Farmer: *J. Phys. D*, 1995, **28D**, 2089
9. A. M. Makara: *Automat. Weld.*, 1997, **30**, (9), 1.
10. K. Hiraoka, A. Okada and M. Inagaki: *Q. J. Jpn Weld. Soc.*, 1985, **3**, (2), 241.
11. K. Yamamoto, M. Tanaka, S. Tashiro, K. Nakata, K. Yamazaki, E. Yamamoto, K. Suzuki and K. Murphy: *Sci. Technol. Weld. Join.*, 2008, **13**, (6), 566.
12. C. R. Heiple and J. R. Roper: *Weld. J.*, 1982, **61**, (4), 97s.
13. P. Sahoo, T. Debroy and M. J. McNllan: *Met. Trans. B*, 1988, **19B**, 483.
14. M. Tanaka and J. J. Lowke: *J. Phys. D*, 2007, **40D**, R1.